Fermi National Accelerator Laboratory

Increasing Antiproton Yields Via Recirculating Beam Targeting

N. Mokhov and A. Van Ginneken

Fermi National Accelerator Laboratory
P.O. Box 500, Batavia, Illinois 60510

June 1994

Disclaimer

Increasing Antiproton Yields
via
Recirculating Beam Targeting

N. Mokhov and A. Van Ginneken

Fermi National Accelerator Laboratory*

P. O. Box 500, Batavia, IL 60510

June 1994

Abstract

Targetry aspects of a $\bar{p}$ production scheme using a recirculating beam are presented. Results show that $\bar{p}$ yield may be increased more than a full order of magnitude over that of presently adopted single-turn thick targets, while energy deposition and beam heating may be kept below reasonable limits. Collection of the produced $\bar{p}$, which may require a novel approach for this scheme, is not addressed here.

1 Introduction

In almost all realistic Tevatron upgrade scenarios—which retain the $\bar{p}p$ option—increased luminosity requires increased $\bar{p}$ production. This is especially true if larger rings are contemplated to increase the energy of the collision. Present $\bar{p}$ targets operate near their limits determined by structural stability so that even the higher intensities from anticipated Main Injector (MI) operation pose a problem. These targets also waste a large fraction of the protons: those traversing it without interaction and those interacting well away from the $\bar{p}$ focus where collection efficiency is low.

This note examines a different $\bar{p}$ production scheme: following acceleration to the desired energy (assumed to be 120 GeV) MI beam is repeatedly

---

1

circulated through a bypass which houses a *thin* target along with the necessary focusing elements for both proton beam and produced $\bar{p}$s. In addition the bypass must contain absorbers which intercept the resulting radiation and reduce it to acceptable levels. This note is limited to a discussion of the targetry aspects of this scheme. The rest of it may well pose grave—even insurmountable—technical difficulties but since targeting is at the very basis of this proposal it is best to examine it first.

Some of the merits of this scheme are immediately obvious: a *thin* target avoids all depth-of-focus problems and recirculation allows virtually the entire beam to be utilized. Cascade buildup in the target is minimal which suppresses energy deposited as well as induced radioactivity. This may be further suppressed by using low-Z targets: in the conventional scheme the main advantage of high-Z targets is their high density to reduce the depth-of-focus problems which are no longer an issue here. In addition one can employ a moving target and take advantage of the multiple turns and the proton revolution time in MI to dilute the energy deposition density. Neglecting the bypass this is about 11 μsec which—stretched over a large number of turns—translates into considerable dilution even in a slow moving target.

Among the problems not addressed here the most critical one is likely to be compression of the large longitudinal phase space into which the $\bar{p}$ are generated. Also not addressed are matching the bypass to MI and the design of p and $\bar{p}$ focusing systems. The latter should avoid interposing more material, such as lithium lenses, in the beam which would likely have more of a detrimental effect on the protons than can be justified by enhanced $\bar{p}$ collection. In this scheme the target and its surroundings essentially act as a dump for the MI beam. There are advantages to this since almost the entire beam interacts in the target, which results in very effective dispersal of the resulting cascades if the absorbers are placed some distance away. Nonetheless, a serious design of this 'dump' and its integration with the focusing system is likely to pose some problems as well. Elastically scattered protons tend to stay with the beam for considerable distances before being swept out of the aperture. Any problems connected with this are best studied by means of simulations comprising both MI and bypass. It is unlikely that such problems will be of paramount importance in this scheme.

Below, in sec. 2 the impact of this scheme on the MI cycle is examined. Sec. 3 addresses emittance growth of the beam due to repeated target traversal. Sec. 4 compares $\bar{p}$ production in various targeting schemes as well as with more conventional ones. Some calculated results on energy deposition in these targets are presented in sec. 5. Conclusions are in sec. 6.

2

2 Main Injector Cycle

First of all a rough estimate is needed of optimum time spent on $\bar{p}$ production as part of the acceleration cycle. Let $r_{\bar{p}}$ represent the number of $\bar{p}$s produced per proton in a thin target of unit thickness which lie within the acceptance of the $\bar{p}$ collection system, N_p the number of protons accelerated per cycle $(3 \cdot 10^{13})$, Δ target thickness, and λ collision length of the material. The number of acceptable $\bar{p}$s produced during the $(n + 1)^{th}$ traversal is

$$N_p r_{\bar{p}} \lambda \left(1 - e^{-\frac{\Delta}{\lambda}}\right) e^{-n\frac{\Delta}{\lambda}}. \tag{1}$$

For a large enough number of turns the total yield per cycle may be approximated by summing eq.(1) over n from 0 to ∞:

$$\text{yield per MI cycle} \approx \lambda N_p r_{\bar{p}}. \tag{2}$$

Let τ_a represent acceleration time (1.5 sec for MI) and τ_c coasting time dedicated to $\bar{p}$ production such that $\tau_c = n\tau_0$ where n is the number of turns and $\tau_0 \approx 11\mu sec$ is the revolution time. Beyond some number, n_c, of orbits it becomes advantageous to dump the remaining proton beam and start a new MI cyle. This occurs when $\bar{p}$ production during the n_c^{th} revolution, eq.(1) divided by τ_0 and using $\Delta \ll \lambda$, falls below that averaged over the entire MI cycle, i.e., when

$$\frac{N_p r_{\bar{p}} \Delta e^{-n_c \frac{\Delta}{\lambda}}}{\tau_0} = \frac{\lambda N_p r_{\bar{p}}}{\tau_a + \tau_c} \approx \frac{\lambda N_p r_{\bar{p}}}{\tau_a} \tag{3}$$

leading to

$$n_c = \frac{\lambda}{\Delta} \ln \frac{\tau_a \Delta}{\tau_0 \lambda}. \tag{4}$$

Table I shows n_c and τ_c, in seconds, for various choices of target thickness.

Table I *Optimum Traversals*

Δ/λ	n_c	τ_c
0.0001	26130	0.29
0.001	4915	0.054
0.01	722	0.0079
0.1	95	0.00105

Total thickness traversed (in units of λ) is obtained by multiplying columns 1 and 2 of Table I and ranges from 2.6 to 9.5 collision lengths so that indeed almost all of the beam interacts thus justifying eq.(2). Except for the first row the condition $\tau_c \ll \tau_a$, implied in eq.(3), is easily satisfied.

3

The above discussion assumes constant target thickness. For a moving target, an alternative is to have its thickness increase exponentially at a rate such that $\bar{p}$ production remains constant over successive traversals. This would require very precise timing between accelerator and the target driving device. As long as energy deposition from cascade buildup remains small compared to that due to the beam particles, such variable thickness targets provide more uniform energy deposition as well. To keep $\bar{p}$ production constant during τ_c, target thickness, Δ_k, as a function of revolution number, k, must satisfy

$$\left(1 - e^{-\frac{\Delta_1}{\lambda}}\right) = e^{-\sum_{i=1}^{k-1}\Delta_i/\lambda}\left(1 - e^{-\frac{\Delta_k}{\lambda}}\right).$$ (5)

After some number ℓ of revolutions

$$e^{-\sum_{i=1}^{\ell-1}\Delta_i/\lambda} < \left(1 - e^{-\frac{\Delta_1}{\lambda}}\right)$$ (6)

so that Δ_ℓ can never be thick enough to satisfy eq.(6) which thus limits the number of traversals. In practice, considerations of target heating and demands on the device driving the target are likely to override eq.(6). A moving target with, e.g., linearly increasing thickness may be a useful compromise.

3 Emittance Growth

In this section the effects on the *proton beam* passing repeatedly through a thin target are discussed. The main effects are (transverse) emittance growth due to multiple Coulomb scattering counteracted by (transverse) cooling due to ionization losses along with absorption due to inelastic prosesses— of which $\bar{p}$ production is a tiny part. As mentioned above, nuclear elastic processes are not treated explicitly. For now, they are simply included in the total cross section even though a significant fraction is expected to remain with the beam for multiple turns and thus to contribute to $\bar{p}$ production.

If a small RF field makes up for average momentum lost in the target then some damping of transverse motion results because momentum is lost in all three directions (proportional to projected pathlength in the absorber) but is only restored along the beam direction. At some level of approximation multiple scattering and ionization cooling combine into a differential

equation (see e.g. [1]):

$$\frac{d\epsilon_T}{dn} = -\frac{dE}{dx}\frac{\Delta}{E_0}\epsilon_T + \frac{\beta}{2}\left(\frac{0.014}{E_0}\right)^2\frac{\Delta}{L_R} \tag{7}$$

which is the change in transverse emittance (ϵ_T) per turn, where E_0 represents beam energy (in GeV), L_R target radiation length, dE/dx energy loss per unit length, and β betatron wavelength at the target position. The solution of eq.(7), with $\epsilon_T(0)$ the transverse emittance before the first target traversal, is

$$\epsilon_T(n) = \epsilon_T(0)e^{-\frac{dE}{dx}\frac{\Delta}{E_0}n} + \frac{\beta}{2}\frac{(0.014)^2}{E_0 L_R}\frac{1}{\frac{dE}{dx}}\left(1 - e^{-\frac{dE}{dx}\frac{\Delta}{E_0}n}\right). \tag{8}$$

Note that in eq.(8) the argument of the exponential is the fractional energy loss in the target which, for the number of turns as per Table I, is always small so that eq.(8) essentially reverts back to eq.(7):

$$\epsilon_T(n) = \epsilon_T(0) + \left(\frac{\beta}{2}\left(\frac{0.014}{E_0}\right)^2\frac{\Delta}{L_R} - \epsilon_T(0)\frac{dE}{dx}\frac{\Delta}{E_0}\right)n. \tag{9}$$

From eq.(8) (when $n \to \infty$) or directly from eq.(7) an equilibrium emittance is readily obtained:

$$\epsilon_T^{eq} = \frac{\beta}{2}\frac{(0.014)^2}{E_0\frac{dE}{dx}L_R}. \tag{10}$$

The normalized (Fermilab convention) design emittance for MI is 20π mm-mrad. This translates to an rms emittance of $8.2 \cdot 10^{-8}$ m-rad at 120 GeV. Equilibrium emittances from eq.(10) range from $7.4 \cdot 10^{-6}\beta$ for beryllium to $1.0 \cdot 10^{-4}\beta$ for tungsten. As a result, unless β is very small, there is net beam heating while for optimum traversals (as per Table I) the emittance is expected to remain well below ϵ_T^{eq} at all times. Table II displays some needed parameters for four standard materials adopted throughout this note. Note that λ here includes nuclear elastic scattering while the column marked λ_{abs} is the more common absorption length. At the present level of approximation proton removal from the beam scales as λ^{-1} while $\bar{p}$ production goes (roughly) as λ_{abs}^{-1}.

Table II Material Parameters				
Param	L_R	dE/dx	λ	λ_{abs}
units	g/cm^2	MeV·cm^2/g	g/cm^2	g/cm^2
Be	65.19	2.028	55.8	78.5
Al	24.01	2.177	70.6	108.5
Cu	12.86	1.955	85.6	138.4
W	6.76	1.659	110.3	193.2

From eqs.(8 or 9) and for a reference β of 1 meter one readily obtains for the numerical emittance growth

$$
\begin{aligned}
\epsilon_T(n) &= 8.2 \cdot 10^{-8} + 5.7 \cdot 10^{-9} n\Delta/\lambda \quad (Be) \\
&= 8.2 \cdot 10^{-8} + 1.1 \cdot 10^{-7} n\Delta/\lambda \quad (W)
\end{aligned} \tag{11}
$$

Table III lists final emittances (in mm-mrad) after an optimum number of revolutions, n_c, (Table I) starting from an initial $\epsilon_T(0) = 0.082$ mm-mrad and for β=1 m.

Table III *Emittance Growth*

Δ/λ	0.0001	0.001	0.01	0.1
$n_c\Delta/\lambda$	2.61	4.91	7.22	9.50
Target	Final Emittance after n_c Turns			
Be	0.097	0.110	0.123	0.137
Al	0.134	0.180	0.226	0.271
Cu	0.200	0.304	0.408	0.511
W	0.372	0.628	0.883	1.140

As can be seen emittance growth appears quite tolerable and remains well below the admittance determined by MI aperture. If necessary, the proton focusing system could provide compensation for growth in beam size. If emittance growth is expressed as a function of total target thickness traversed rather than number of traversals then the above analysis applies equally well to the variable thickness case. Eq.(7) represents only the average behavior of the proton beam. In reality one deals with a 'first passage' problem: large angle—Coulomb or nuclear—scattering causes particles to be lost from the beam or to become part of the 'tails' of the emittance. To study all of this in more detail one must resort to simulations.

Changes in longitudinal emittance are expected to be much smaller than transverse ones if a small restoring RF field is applied. Some protons will be lost from the RF-bucket due to large angle scattering off atomic electrons

and due to straggling of the energy loss distribution. In gross numbers such losses are overshadowed by those due to nuclear inelastic events. Again for a serious design a more precise study of where and how they are lost from the beam can be made part of a more detailed simulation.

4 Antiproton Production

Antiproton production for thick targets has been studied [2, 3] with the aid of Monte Carlo calculations augmented with a model for $\bar{p}$ production in particle-nucleus interactions. For the present purpose, this work must be extended to include thinner targets and lower-Z materials. This is done with the MARS program [3, 4]. MARS provides good agreement with observations at Fermilab which is essential in lending validity to the conclusions reached here. However, in this study it is more the intercomparison of the relative magnitude of the results which is emphasized and any remaining discrepancies will tend to cancel out in such a comparison.

Results are presented for the same materials and target thicknesses (excluding the $\Delta/\lambda{=}0.0001$ case) as explored in the previous sections and for a set of three beam dimensions (assumed to be an uncorrelated bi-Gaussian): $\sigma_x = \sigma_y{=}$ 0.05, 0.1, and 0.3 mm. This is contrasted with production in a thick target ($\Delta/\lambda{=}0.8$). Antiproton collection is treated the same as in [3]: $\bar{p}$s with a momentum of 8.9 GeV/c ($\pm 2\%$) are collected within an acceptance of 20π mm-mrad with a maximum angular divergence (at the end of the target) of 90 mrad. This corresponds roughly to the acceptance for the present Fermilab $\bar{p}$-target and is adopted in this study to facilitate comparison with past achievements—even though collection may be different for a recirculating beam.

Table IV lists the $\bar{p}$ (single turn) yields per incident proton for the above set of target parameters. Results for $\sigma{=}0.1$ mm are also shown in graphical form in fig. 1a while 1b displays corresponding graphs for an acceptance of 40π mm-mrad. Figs. 2a–c show more detailed variation of yield with beam size, acceptance, and maximum divergence angle for the case of a beryllium target of thickness $\Delta/\lambda{=}0.01$. As can be seen, for thin targets low-Z materials offer considerable advantage as does small beam size. The latter also means a low β at the target which results in less beam heating but higher maximum energy deposition.

7

Table IV Yield of $\bar{p}$ per Incident Proton (Single Turn)					
Target	σ (mm)	$\Delta/\lambda = 0.001$	$\Delta/\lambda = 0.01$	$\Delta/\lambda = 0.1$	$\Delta/\lambda = 0.8$
thickness (cm)		0.030	0.30	3.0	
Be	0.05	$3.22 \cdot 10^{-7}$	$3.24 \cdot 10^{-6}$	$1.44 \cdot 10^{-5}$	
	0.1	$2.87 \cdot 10^{-7}$	$2.88 \cdot 10^{-6}$	$1.38 \cdot 10^{-5}$	
	0.3	$1.10 \cdot 10^{-7}$	$1.18 \cdot 10^{-6}$	$9.04 \cdot 10^{-6}$	
thickness (cm)		0.026	0.26	2.6	
Al	0.05	$2.71 \cdot 10^{-7}$	$2.72 \cdot 10^{-6}$	$1.30 \cdot 10^{-5}$	
	0.1	$2.42 \cdot 10^{-7}$	$2.44 \cdot 10^{-6}$	$1.24 \cdot 10^{-5}$	
	0.3	$9.65 \cdot 10^{-8}$	$9.54 \cdot 10^{-7}$	$7.58 \cdot 10^{-6}$	
thickness (cm)		0.0096	0.096	0.96	7.68
Cu	0.05	$2.08 \cdot 10^{-7}$	$2.37 \cdot 10^{-6}$	$1.81 \cdot 10^{-5}$	$3.34 \cdot 10^{-5}$
	0.1	$1.86 \cdot 10^{-7}$	$2.11 \cdot 10^{-6}$	$1.63 \cdot 10^{-5}$	$3.07 \cdot 10^{-5}$
	0.3	$7.36 \cdot 10^{-8}$	$8.06 \cdot 10^{-7}$	$7.41 \cdot 10^{-6}$	$2.42 \cdot 10^{-5}$
thickness (cm)		0.0057	0.057	0.57	4.56
W	0.05	$1.77 \cdot 10^{-7}$	$1.96 \cdot 10^{-6}$	$1.76 \cdot 10^{-5}$	$3.65 \cdot 10^{-5}$
	0.1	$1.59 \cdot 10^{-7}$	$1.77 \cdot 10^{-6}$	$1.55 \cdot 10^{-5}$	$3.55 \cdot 10^{-5}$
	0.3	$5.85 \cdot 10^{-8}$	$6.69 \cdot 10^{-7}$	$6.27 \cdot 10^{-6}$	$2.55 \cdot 10^{-5}$

Table V Yield of $\bar{p}$ per MI Cycle					
Target	σ (mm)	$\Delta/\lambda = 0.001$	$\Delta/\lambda = 0.01$	$\Delta/\lambda = 0.1$	$\Delta/\lambda = 0.8$
thickness in cm		0.030	0.30	3.0	
Be	0.05	$9.7 \cdot 10^{9}$	$9.7 \cdot 10^{9}$	$4.3 \cdot 10^{9}$	
	0.1	$8.6 \cdot 10^{9}$	$8.6 \cdot 10^{9}$	$4.1 \cdot 10^{9}$	
	0.3	$3.3 \cdot 10^{9}$	$3.5 \cdot 10^{9}$	$2.7 \cdot 10^{9}$	
thickness in cm		0.026	0.26	2.6	
Al	0.05	$8.1 \cdot 10^{9}$	$8.2 \cdot 10^{9}$	$3.9 \cdot 10^{9}$	
	0.1	$7.3 \cdot 10^{9}$	$7.3 \cdot 10^{9}$	$3.7 \cdot 10^{9}$	
	0.3	$2.9 \cdot 10^{9}$	$2.9 \cdot 10^{9}$	$2.3 \cdot 10^{9}$	
thickness in cm		0.0096	0.096	0.96	7.68
Cu	0.05	$6.2 \cdot 10^{9}$	$7.1 \cdot 10^{9}$	$5.4 \cdot 10^{9}$	$1.00 \cdot 10^{9}$
	0.1	$5.6 \cdot 10^{9}$	$6.3 \cdot 10^{9}$	$4.9 \cdot 10^{9}$	$9.2 \cdot 10^{8}$
	0.3	$2.2 \cdot 10^{9}$	$2.4 \cdot 10^{9}$	$2.2 \cdot 10^{9}$	$7.3 \cdot 10^{8}$
thickness in cm		0.0057	0.057	0.57	4.56
W	0.05	$5.3 \cdot 10^{9}$	$5.9 \cdot 10^{9}$	$5.3 \cdot 10^{9}$	$1.18 \cdot 10^{9}$
	0.1	$4.8 \cdot 10^{9}$	$5.3 \cdot 10^{9}$	$4.7 \cdot 10^{9}$	$1.15 \cdot 10^{9}$
	0.3	$1.74 \cdot 10^{9}$	$2.0 \cdot 10^{9}$	$1.88 \cdot 10^{9}$	$7.7 \cdot 10^{8}$

In Table V results of Table IV are converted to $\bar{p}$s produced per MI cycle

using the design value of $3 \cdot 10^{13}$ protons per cycle and eq.(2) corrected for finite number of turns of coasting, n_c, as per Table I. Entries corresponding to $\Delta/\lambda = 0.8$ assume a single turn. Table V illustrates the potential gain of a recirculating scheme. By using smaller beams and low-Z targets impressive gains—exceeding an order of magnitude—in $\bar{p}$ production per MI cycle are possible compared with the present system as exemplified by a copper target of $\Delta/\lambda = 0.8$ and a beam σ of 0.3 mm.

5 Energy Deposition

Calculation of energy deposition for some of the beam-target geometries has likewise been performed with MARS. In the thin target regime maximum energy deposition is to good approximation derivable solely from ionization energy losses of the primary beam. For a bi-Gaussian distribution

$$\rho_E^{max} = \frac{dE/dx}{2\pi\sigma_x\sigma_y}. \tag{12}$$

If dE/dx is expressed in GeV·cm^2/g (0.001 times the Table II entries [5]) and σ_x, σ_y in cm, then eq.(12) gives the maximum energy density in GeV/gram. From the energy deposition one may derive an 'instantaneous' temperature rise of the target, i.e., before any heat exchange takes place.

Beyond this matters become more complicated: for a stationary target heat is added with each successive traversal and then redistributed to other parts of the target—with or without measures taken to cool the assembly. In a serious design study the distribution of energy deposition along with the information about timing and intensity of a series of traversals can be used to study heating/cooling cycles in full detail as well as to address concerns about structural stability of the target.

In a moving target energy deposition is diluted along the direction of motion. If this is, e.g., the x-direction then σ_x in eq.(12) is replaced by $D_x + \sigma_x$, where D_x is the distance the target moves between traversals

$$\rho_E^{max} = \frac{dE/dx}{2\pi\,(D_x + \sigma_x)\,\sigma_y}. \tag{13}$$

Table VI collects some results related to energy deposition (for the $\Delta/\lambda=0.01$ targets, although it depends little on thickness). Maximum energy deposition per incident proton as calculated by MARS and by eq.(12) is included and MARS results are also shown graphically in fig. 3. This can

be translated into an instantaneous temperature rise for one turn of full MI beam on a stationary or moving target. Results presented for the latter assume, by way of illustration, an arbitrary—but convenient—target speed of 100 m/sec. The ΔTs in Table VI are calculated with an initial temperature of 100 °C and assume that no phase change takes place—which is also desirable from an operational point of view—so that they are correct only below the respective melting points. Above that the ΔT remain a good indication of the magnitude of the problem. To good approximation the ΔT scale linearly with beam intensity.

Table VI Energy Deposition and Temperature Rise					
Target	σ (mm)	ρ_E^{max} GeV/g·p MARS	ρ_E^{max} GeV/g·p eq.(12)	ΔT °C/turn stat. tgt	ΔT °C/turn moving
Be	0.05	15.3	12.6	20 600	1 090
	0.1	3.71	3.22	5 150	562
	0.3	0.416	0.359	730	181
Al	0.05	14.0	13.9	61 900	2 720
	0.1	3.49	3.46	15 500	1 310
	0.3	0.391	0.384	1 750	394
Cu	0.05	12.0	12.4	117 000	5 180
	0.1	3.01	3.11	29 300	2 540
	0.3	0.350	0.346	3 510	830
W	0.05	9.10	10.6	273 000	11 900
	0.1	2.39	2.64	71 800	5 980
	0.3	0.295	0.294	8 870	1 900

6 Concluding Remarks

By way of example consider the case of a moving beryllium target 0.3 cm thick ($\Delta/\lambda=0.01$) and a beam of $\sigma=0.1$ mm. Antiproton production for this case exceeds that for a conventional thick ($\Delta/\lambda=0.8$) target with single-turn irradiation by about a factor of 12. The temperature rise (562°C) appears tolerable and should keep the target from melting (at 1280°C) or from undergoing severe structural changes. For the smaller beam of $\sigma=0.05$ mm the gain would be slightly higher (13.5) but here ΔT is more worrisome. It is also evident from fig. 2a that little is to be gained in $\bar{p}$ yield with yet smaller σ. For the proton beam in this example $\sigma=0.1$ mm means $\beta=0.38$ m at the target which should be easily achievable. After 722 turns (n_c as per Table

I) emittance growth is less than 20% which can either be tolerated or be compensated for.

The large increase in $\bar{p}$s arises because virtually the entire beam interacts and each interacting proton contributes maximally to $\bar{p}$ production because a thin target can be placed precisely at the focus of the collection device. Targeting-wise eq.(2), which is a good approximation to the recirculating thin target case, represents an essentially unassailable upper limit to $\bar{p}$ production. By contrast in a thick target about half the protons do not interact. Of those that do, most interact in regions unfavorable for collection which accounts for a factor of three (see fig. 12 of [2]) and all are reduced another factor of two due to absorption of both p and $\bar{p}$s. Altogether this rough accounting readily explains the above mentioned factor of $\sim$12.

Many practical questions remain to be explored. A problem specific to the targetry aspects is that of operating a high speed moving target in an evacuated region. In this respect carbon might be a better choice than beryllium. Carbon has a higher melting point (3550°—but a sublimation point of 3367°C) than beryllium though a lower specific heat (0.17 cal/g for carbon vs 0.436 for beryllium at room temperature). Certain forms of graphite have excellent mechanical and thermo-conductive properties. A gaseous target would avoid many questions—such as about structural stabilty—though it may be difficult to make such a target thin enough to avoid depth-of-focus problems yet thick enough (in terms of Δ/λ) to keep coasting times to a reasonable fraction of the MI cycle. Beam sweeping—also facilitated by multiple turns—may be considered as an alternative (or an addition) to a moving target.

Antiproton production with a thin target in a recirculating beam appears to have the potential to increase $\bar{p}$ yields by about one order of magnitude. Many problems remain to be studied. If these can be satisfactorily resolved, the cost of such a project seems quite reasonable. Since it is unlikely that the bypass can be located in the MI enclosure some civil construction would be required. Even so the cost for this would be only a modest fraction of the MI civil construction expenses. The same probably applies to the cost of magnets and other components. If so, this could well be a cost-effective way to score an impressive gain in $\bar{p}$ yield and consequently in Tevatron luminosity. Similar gains may apply elsewhere as well as for other targeting applications such as a fixed target $\bar{p}$-beam—for which the time structure imposed by the recirculation may actually offer some advantages.

11

Acknowledgements Our thanks to C. Ankenbrandt, N. Gelfand and J. Marriner for their comments.

References

[1] D. Neuffer, Particle Accelerators 14, 75 (1983).

[2] C. Hojvat and A. Van Ginneken, Nucl. Inst. Meth. 206, 67 (1983).

[3] I.L. Azhgirey, N.V. Mokhov, and S. I. Striganov, FNAL-TM-1730 (1991).

[4] N. Mokhov, MARS10 *Code System User's Guide*, FNAL-FN-509 (1989); —, MARS12 *Code System*, Proc. SARE Workshop, Santa Fe (1993).

[5] For a thin target the dE/dx in eq.(12) should be the *restricted dE/dx* to account for δ-rays which may leave the target. There will also be a correction—of opposite sign—due to nuclear recoil and charged evaporation particles following nuclear interaction.
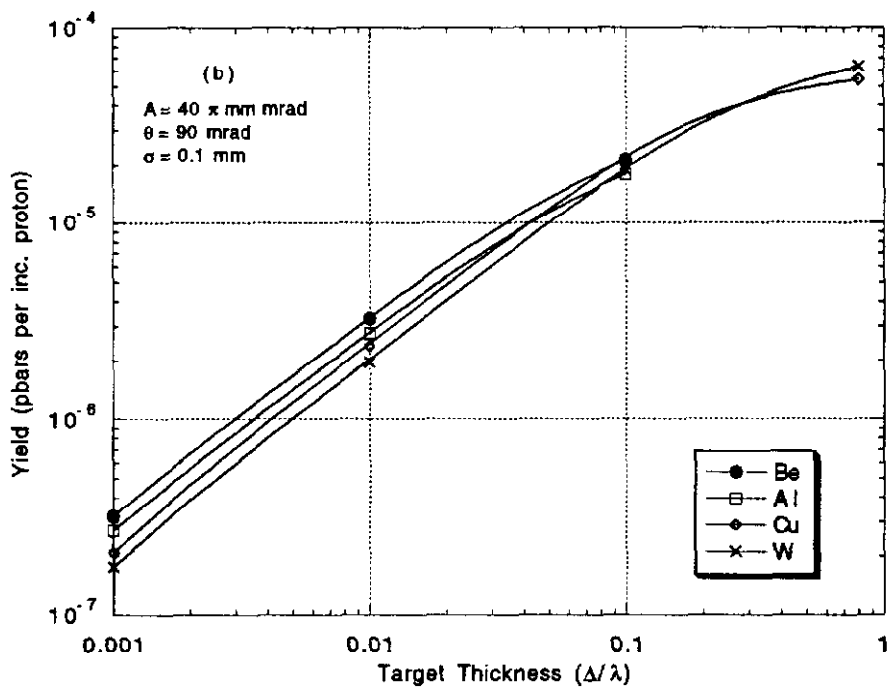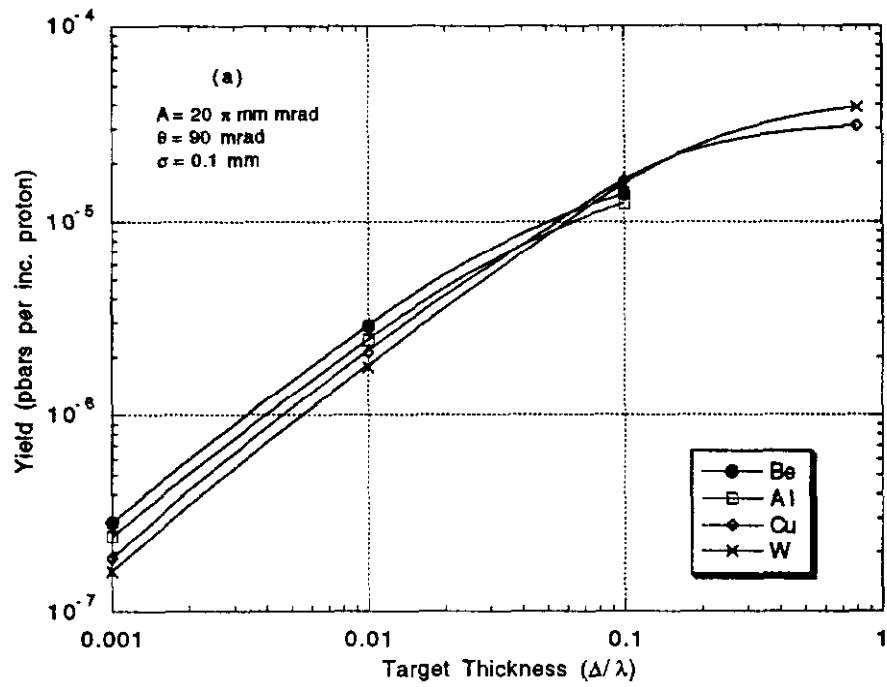
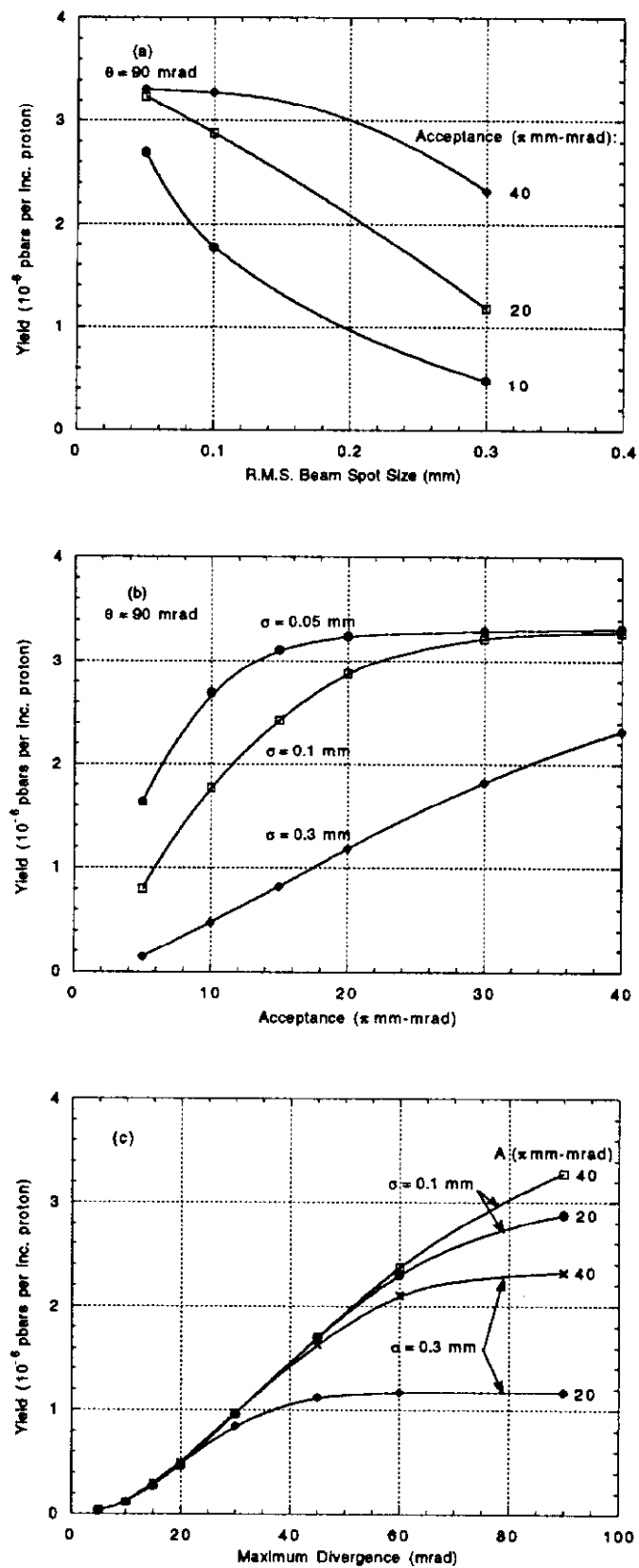Fig. 1. Antiproton yield as a function of target thickness

Fig. 2. Antiproton yield from Be target of $\Delta/\lambda = 0.01$ thick versus (a) beam size, (b) acceptance, and (c) maximum angular divergence
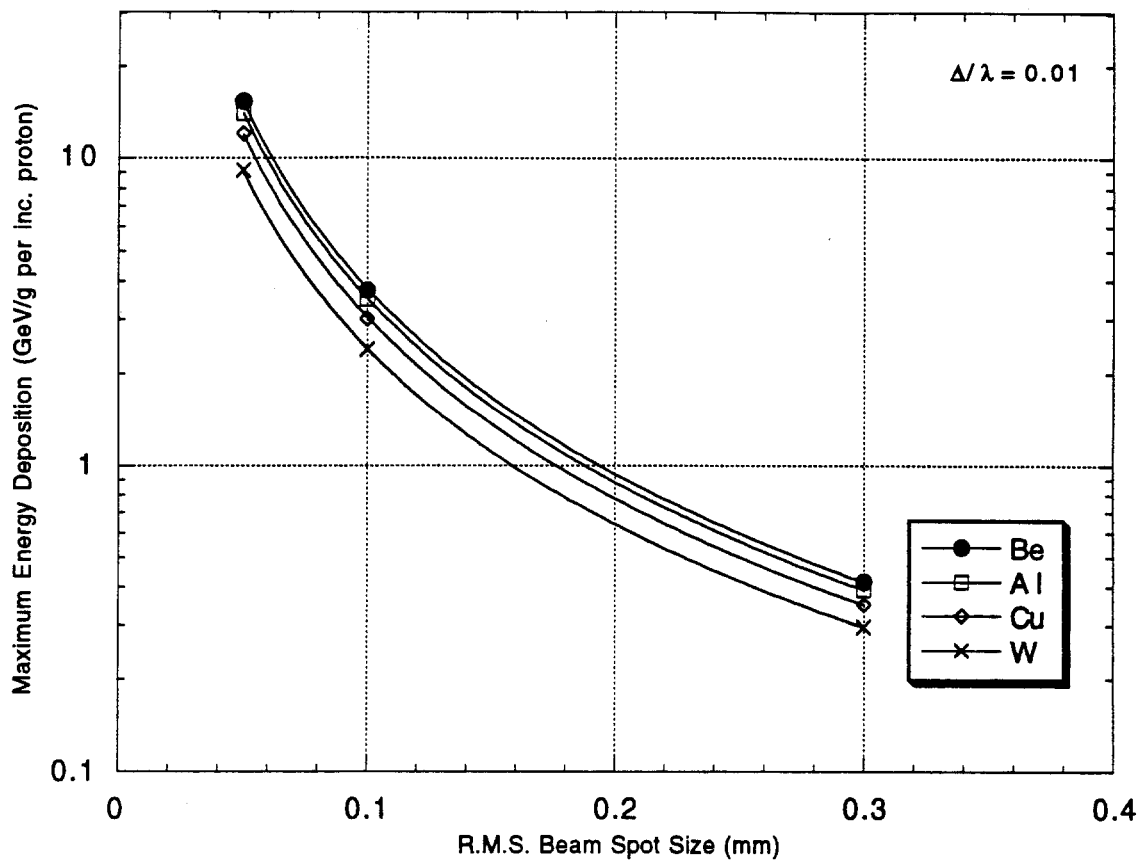
Fig. 3. Maximum energy deposition versus beam size